URSI GASS 2020, Rome, Italy, 29 August - 5 September 2020

Interference Mitigation for Synthetic Aperture Radar Data using Tensor Representation and Low-Rank Approximation

Mingliang Tao(1), Jieshuang Li(1), Jia Su(1), Yifei Fan(1), Ling Wang(1)*, Zijing Zhang(2)
(1) School of Electronics and Information, Northwestern Polytechnical University, 710072 Xi'an, China
(2) School of Electronic Engineering, Xidian University, 710071 Xi'an, China

Abstract

Radio frequency interference (RFI) is a critical issue to synthetic aperture radar (SAR), which would cause great distortions to amplitude and phase information of the received echoes. Most of the existing literatures deal with the interference separation problem in time domain, frequency domain, or time-frequency domain using the matrix representation and matrix optimization tools, without further exploiting the correlation among multiple dimensional measurements. This paper proposes an interference separation for SAR data using tensor representation by formulating a novel time-frequency-azimuth tensor. Then, the low-rank property of the interference is utilized and the interference contribution is estimated using low rank tensor approximation. Experimental results demonstrate that the interference components is effectively extracted, and well imaging results could be recovered.

1 Introduction

The contest among various radio services against the finite electromagnetic spectrum are making the electromagnetic environment more and more congested. Synthetic aperture radar (SAR) requires larger bandwidth to obtain finer resolution, and thus easily affected by radio emitters sharing the same frequency band, which is referred to as the radio frequency interference (RFI) [1].

The presence of strong RFI would cause great distortions to the signal characteristics of the echo, such as the amplitude, phase, frequency, and polarization [2]. It not only would increase the difficulty of image formation process, but also would present as haze-like artifacts in the SAR image. Moreover, it will degrade the interpretation accuracy using incorrect imaging result, such as the target detection, information extraction, and parameters retrieval, etc. Therefore, it is of great importance to improve characterization of the RFI environment and seek an effective way to mitigate the adverse impacts on the SAR echoes [3-7].

SAR system with multiple antennas provides additional degree of freedom to suppress the RFI from spatial directions. Its basic idea is using array beam-forming techniques to orient pattern nulls towards sources of RFI. Bollian *et al.* [3] proposed using digital beamforming techniques for the 32-channel EcoSAR system. The merit of spatial filtering is that it is applicable to the cases that the RFI and SAR signals come from different spatial directions, independent of the RFI signal types. These multichannel-based methods are effective to remove interference, but will also increase the complexity of SAR system and cannot be applied to existing mono-channel SARs without an update of the hardware structure.

For single channel SAR system, the post-processing mitigation is applied. Current RFI mitigation techniques work best for interfering signals that have sparse spectral or temporal or spectral-temporal occupancy with the target echoes. Su *et al.* proposed using robust principle component analysis in time-frequency domain [4]. Li *et al.* [5] utilized the sparse property to recover the useful echoes. Fan *et al.* [6] proposed using advanced deep learning techniques in time-frequency domain. Above mentioned methods deal with the interference separation problem in time domain, frequency domain, or time-frequency domain using the matrix representation and matrix optimization tools. Huang *et al.* firstly characterize the echoes in a novel 3-D range-azimuth-space tensor model by dividing the azimuth into several sub-blocks, and the interference is suppressed by solving the tensor optimization problem [7]. Tensor algebra extends the mathematical definitions into higher-dimensional space, and is very suitable for characterizing data with coupling correlation among multiple dimensions.

This paper proposed a novel tensorial representation of the echoes by constructing a 3-D (range) time-frequency-azimuth tensor model. The low-rank characteristics of the interference along each mode is verified. Then, a separation scheme is exploited by applying the low rank approximation. The optimization is realized by incorporating the spatial correlation between time-frequency measurements and the variation among spatial samples. The energy contribution of the interferences could be extracted and excised.

2 Signal Model and Methodology

2.1 Basic Mathematical Notations

A *tensor* is defined as a multi-dimensional array, and its number of dimensions is referred to as *mode* or *order*. The tensor definition unifies the framework for depicting the

data. Scalar, vector and matrix are special cases of the tensor, with the mode of 0, 1 and 2, respectively. Scalars are denoted by lowercase letters, e.g., x; vectors are denoted by boldface lowercase letters, e.g., $\mathbf{x}$; matrices by boldface capital letters, e.g., $\mathbf{X}$. For simplicity, only the third-order tensor is considered throughout the paper, which is denoted by Euler script letters, i.e., $\mathcal{X} \in \mathbb{C}^{I_1 \times I_2 \times I_3}$, whose single entry is a complex scalar and expressed as $x_{i_1 i_2 i_3}$, where $1 \le i_n \le I_n (1 \le n \le 3)$ are indexes along each mode. $\mathbf{X}_{(n)}$ is the mode-n matricization of the tensor.

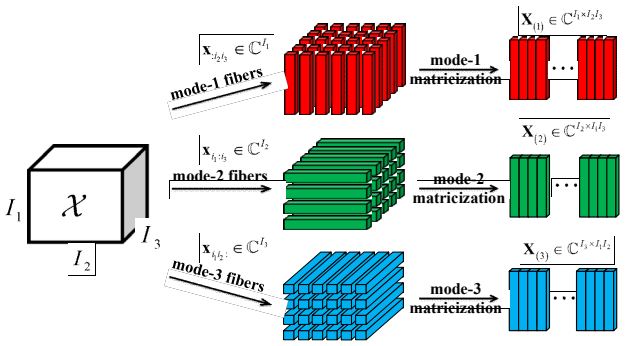

Figure 1. Illustration of the mode- n fibers and its corresponding matricization process.

2.2 Signal Model

Generally, the radar echoes could be expressed as a mixture of target echoes, interference from the RFI emitter and system additive noise [1], and can be depicted as a 2-D matrix model,

$$\mathbf{X}(\hat{t}, t_m) = \mathbf{S}(\hat{t}, t_m) + \mathbf{I}(\hat{t}, t_m) + \mathbf{N}(\hat{t}, t_m) \quad (1)$$

where the $\mathbf{X}$ denotes the received echoes, $\mathbf{S}$ denotes the useful target echoes, $\mathbf{I}$ denotes the interference, and $\mathbf{N}$ denotes the additive noise. $\hat{t}$ and t_m denotes the range fast-time and azimuth slow-time samples.

(1) Azimuth Correlation

Generally, the interference separation process is realized for each azimuth pulse at each time instant t_m independently. To maximize the interference to signal ratio, it is usually transform the echoes onto the time-frequency domain, i.e., using the short time Fourier transform,

$$\mathbf{X}_{spec}(m,k) = \sum_n x(n) \cdot g(n - mh) \cdot \exp(-j2\pi kn/M) \quad (2)$$

where $\mathbf{X}_{spec}(m,k)$ denotes the STFT, $g(\bullet)$ is the sliding window function, h is the hop size, and M is the window length.

Since adjacent azimuth pulses constitutes the synthetic aperture, it ignores the correlation among the azimuth samples. Fig.2 shows the spectrogram of adjacent azimuth pulses at different slow time instants. The amplitude and frequency of interference may vary at each time instants, while the useful echoes are highly correlated.

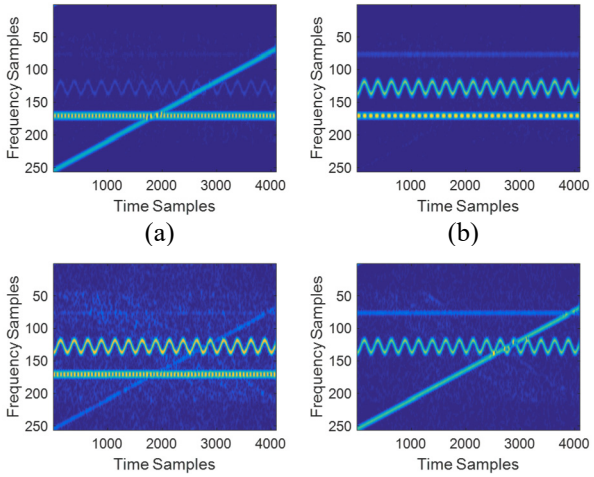

Figure 2. Time-frequency representation of adjacent azimuth pulses at different slow time instants.

Intuitively, it is straightforward to combine these spectrograms together for further processing. Therefore, we propose a novel 3-D (range) time-frequency-azimuth tensor model, which is illustrated in Fig.3. Further, we can extend the 2-D matrix model to

$$\mathcal{X} = \mathcal{S} + \mathcal{I} + \mathcal{N} \quad (3)$$

where $\mathcal{X} \in \mathbb{C}^{I_1 \times I_2 \times I_3}$, $\mathcal{S} \in \mathbb{C}^{I_1 \times I_2 \times I_3}$, $\mathcal{I} \in \mathbb{C}^{I_1 \times I_2 \times I_3}$ and $\mathcal{N} \in \mathbb{C}^{I_1 \times I_2 \times I_3}$ denote the received echoes, useful target echoes, interference, and noise, respectively. The first two dimensions represent the time-frequency representation for each azimuth pulse, and the third mode represents the azimuth spatial dimension.

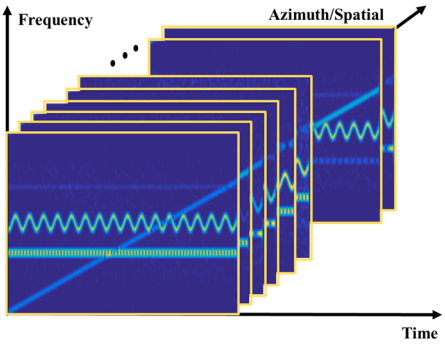

Figure 3. Illustration of 3-D (range) time-frequency-azimuth tensor model.

(2) Low Rank Property

Previous study observed that the time-frequency characteristics of RFI is rather stable [1]. This indicates that the interference would possess the low-rank property, which is widely verified in [4,7]. Fig.3 plots the eigenvalues of the time-frequency-azimuth tensor representation along each mode. In the first two modes, it is observed that the eigenvalues are dominated by a few large values, which indicates the low-rank property is satisfied. The evolvement of the curve for the third mode is not as steep as the first two modes. This may result from

the fact that the existence of spatial correlation among the azimuth samples.

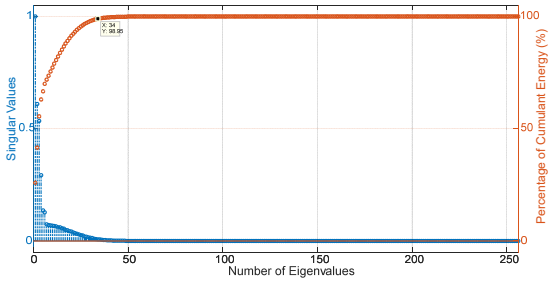

(a)

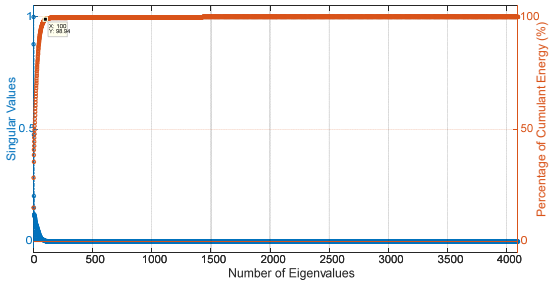

(b)

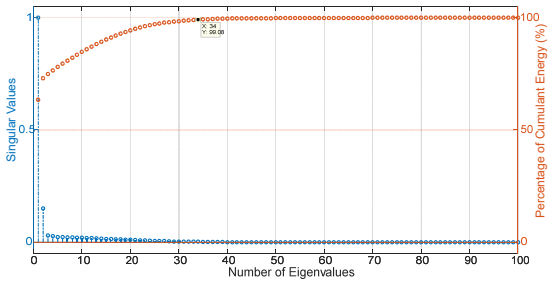

(c)

Figure 4. Eigenvalues of the time-frequency-azimuth tensor representation along each mode.

2.3 Low-rank Approximation

Considering the spatial azimuth correlation and low-rank property of the tensor model, the interference separation problem could be described mathematically as follow.

Given a complex third-order tensor $\mathcal{X} \in \mathbb{C}^{I_1 \times I_2 \times I_3}$, find a tensor $\hat{\mathcal{I}} \in \mathbb{C}^{I_1 \times I_2 \times I_3}$, having rank$_1$ $rank_1\left(\hat{\mathcal{I}}\right) = R_1$, $rank_2\left(\hat{\mathcal{I}}\right) = R_2$, and $rank_3\left(\hat{\mathcal{I}}\right) = R_3$, that minimizes the least squares cost function:

$$\min f\left(\hat{\mathcal{I}}\right) = \left\| \mathcal{X} - \hat{\mathcal{I}} \right\|^2 \tag{3}$$

The low-rank conditions imply that $\hat{\mathcal{I}}$ can be decomposed as

$$\hat{\mathcal{I}} = \mathcal{C} \times_1 \mathbf{U}_{(1)} \times_2 \mathbf{U}_{(2)} \times_3 \mathbf{U}_{(3)} \tag{4}$$

where $\mathbf{U}_{(1)} \in \mathbb{C}^{I_1 \times R_1}$, $\mathbf{U}_{(2)} \in \mathbb{C}^{I_2 \times R_2}$, $\mathbf{U}_{(3)} \in \mathbb{C}^{I_3 \times R_3}$ is the projection matrices, with each have orthonormal columns and $\mathcal{C} \in \mathbb{C}^{R_1 \times R_2 \times R_3}$ denotes the core matrix.

According to [8], the core tensor that optimizes Eq. (3) is given by:

$$\mathcal{C} = \mathcal{X} \times_1 \mathbf{U}_{(1)}^T \times_2 \mathbf{U}_{(2)}^T \times_3 \mathbf{U}_{(3)}^T \tag{5}$$

Equivalently, the minimization problem can be rewritten to a maximization problem,

$$\begin{cases} \max & \left\| \mathcal{X} \times_1 \mathbf{U}_{(1)}^T \times_2 \mathbf{U}_{(2)}^T \times_3 \mathbf{U}_{(3)}^T \right\|^2 \\ s.t. & \mathbf{U}_{(n)}^T \mathbf{U}_{(n)} = \mathbf{I} \end{cases} \tag{6}$$

Basically, the best low-rank approximation problem aims to determine a reduced n-rank tensor $\hat{\mathcal{I}}$ that explains as much of the "energy" (sum of the squared entries) of a given tensor $\mathcal{X}$ as possible under the given constraints.

The optimal solution to $\mathbf{U}^{(n)}$ depend on other projection matrices, and it is rather difficult to solve all the projection matrices simultaneously. Therefore, an alternative least square (ALS) scheme is applied to iteratively solve the projection matrices. In each step, the estimate of one of the matrices $\mathbf{U}^{(n)}$ is optimized, while the other matrix estimates are kept fixed. The merits of this kind of iteration means that the optimization is not processed independently, instead the spatial variation as well as the low-rank property are exploited simultaneously.

After estimating the energy contribution of interference, the useful target echoes could be obtained by excision,

$$\begin{aligned} \hat{\mathcal{S}} &= \mathcal{X} - \hat{\mathcal{I}} \\ &= \mathcal{X} - \mathcal{X} \times_1 \mathbf{U}_{(1)} \mathbf{U}_{(1)}^T \times_2 \mathbf{U}_{(2)} \mathbf{U}_{(2)}^T \times_3 \mathbf{U}_{(3)} \mathbf{U}_{(3)}^T \end{aligned} \tag{7}$$

3 Experimental Results

In this part, we present experimental results by artificially injecting interference into the real measured SAR data. The interference composed of narrow band interference, chirp-modulated wide band interference, and sinusoidal-modulated wideband interference [7], which constitutes a very complicated interference case, as show in Fig.2. The resulting tensor is $\mathcal{X} \in \mathbb{C}^{I_1 \times I_2 \times I_3}$, with $I_1 = 256$, $I_2 = 4096$, and $I_3 = 100$. The estimated rank along each mode is $R_1 = 34$, $R_2 = 100$, and $R_3 = 34$, respectively.

Fig. 5(a)-(d) illustrates the estimated interference components corresponding to Fig.2. It is shown that the evolving structure of the interference is well extracted. Further, Fig. 6 compares the imaging results before and after interference separation. The existence of RFI would affect the imaging process, masking the illuminated area with high noise levels. Fig. 6(b) shows that the illuminated

scene is well recovered after applying the proposed method, in which the target of interest is not masked by distortions.

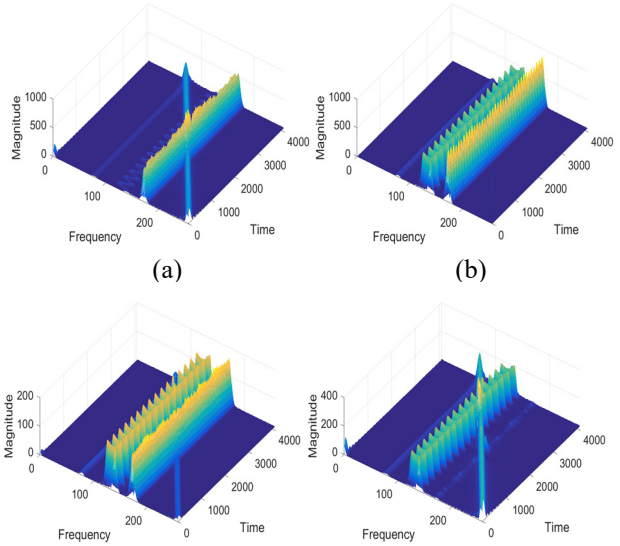

Figure 5. Estimated Interference Components at different specific time instants.

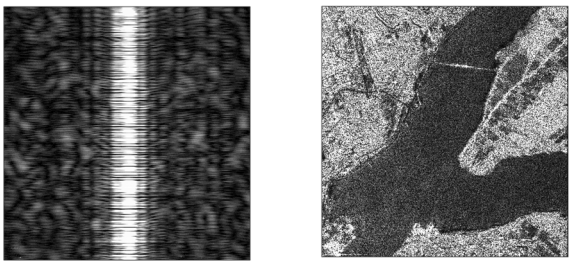

(a) (b)

Figure 6. Imaging results before (a) interference separation and (b) after interference separation.

4 Conclusions

This paper addresses the interference separation of PolSAR data within the tensor algebra framework. A novel 3-D time-frequency-azimuth tensorial representation is proposed, and the low-rank property of the interference is exploited for interference separation by applying the low-rank tensor approximation. The experimental results show the potential of tensor algebra, and more advanced and efficient tensor-based techniques remain to be investigated.

5 Acknowledgements

This work is supported by National Nature Science Foundation of China (NSFC) Grants 61801390, 61701414 and 61901377. This work was also supported by China Postdoctoral Science Foundation under Grant 2018M631123, 2017M623240, and partly supported by Postdoctoral Innovation Talent Support Program under grant BX201700199. This work was also supported by Shanghai Aerospace Science and Technology Innovation Fund under Grant No. SAST2018-041.

6 References

1. P. De Matthaeis, R. Oliva, Y. Soldo, "Spectrum management and its importance for microwave remote sensing," *IEEE Geosci. Remote Sens. Mag.*, 2018, 6, 17–25. doi:10.1109/MGRS.2018.2832057.

2. M. Tao, J. Su, Y. Huang and L. Wang, "Mitigation of radio frequency interference in synthetic aperture radar data: current status and future trends," *Remote Sens.*, 2019, 11(20), 2438, doi: 10.3390/rs11202438.

3. T. Bollian, B. Osmanoglu, R. Rincon, S. Lee, and T. Fatoyinbo, "Adaptive antenna pattern notching of interference in synthetic aperture radar data using digital beamforming," *Remote Sens.*, 2019, 11(11), 1346, doi: 10.3390/rs11111346.

4. J. Su, H. Tao, M. Tao, L. Wang, and J. Xie, "Narrow-band interference suppression via RPCA-based signal separation in time-frequency domain," 2017, 10(11), 5016-5025, doi: 10.1109/JSTARS.2017.2727520.

5. G. Li, W. Ye, G. Lao, S. Kong, D. Yan, "Narrowband interference separation for synthetic aperture radar via sensing matrix optimization-based block sparse Bayesian learning," *Electronics*, 2019, 8, 458, doi: 10.3390/electronics8040458.

6. W. Fan, F. Zhou, M. Tao, X. Bai, P. Rong, S. Yang and T. Tian, "Interference mitigation for synthetic aperture radar based on deep residual network," *Remote Sens.*, 2019, 11(14), 1654, doi: 10.3390/rs11141654.

7. Y. Huang, G. Liao, L. Zhang, Y. Xiang, J. Li, A. Nehorai, "A novel tensor technique for simultaneous narrowband and wideband interference suppression on single-channel SAR system," *IEEE Trans. Geosci. Remote Sensing*, 2019, 57(12), 9575-9588, doi: 10.1109/TGRS.2019.2927764

8. L. De Lathauwer, B. De Moor, and J. Vandewalle, "On the best rank-1 and rank-($R_1, R_2, \ldots, R_N$) approximation of higher-order tensors," *SIAM J. Matrix Anal. Appl.*, 2000, 21(4), 1324-1342, doi: 10.1137/S089547989346995.